TECHNICAL NOTE

An Accurate Dictionary Creation Method for MR Fingerprinting Using a Fast Bloch Simulator

Ryoichi Kose and Katsumi Kose[*]

This study proposes an accurate method for creating a dictionary for magnetic resonance fingerprinting (MRF) using a fast Bloch image simulator. An MRF sequence based on a fast imaging with steady precession sequence and a numerical phantom were used for dictionary generation. Cartesian and spiral readout gradients were used for the Bloch image simulation. The validity and usefulness of the method for accurate dictionary creation were demonstrated by MRF parameter maps obtained by pattern matching with the dictionaries generated by the proposed method.

Keywords: *Bloch simulator, graphics processing unit, magnetic resonance fingerprinting, spiral*

Introduction

Magnetic resonance fingerprinting (MRF) is a novel nuclear magnetic resonance parameter mapping method proposed by Ma et al.[1] Since its proposal, many technical papers concerning pulse sequences,[2] dictionary generation, and matching methods have been published, as well as clinical trials. A number of studies are currently being performed to improve measurement accuracy, speed up data acquisition and processing, and further expand measurement parameters. This research relates to improvement of the dictionary generation closely related to measurement accuracy in MRF.

In general, the entries for the MRF dictionary are T_1, T_2, B_0 (static magnetic field), and B_1^+ (transmission radiofrequency field). For pulse sequences insensitive to B_0 inhomogeneity, such as the fast imaging with steady precession (FISP) sequence, the entries can be reduced into three parameters except B_0. Because the B_1^+ is the external parameter and can be measured by another method such as the Bloch-Siegert method, dictionaries with T_1 and T_2 entries (hundreds of steps, each) are usually calculated for B_1^+ values with relatively few steps (several tens of steps). Therefore, it is essential to calculate the dictionary accurately for T_1 and T_2 entries using the MRF pulse sequence with different B_1^+ parameters.

There are two sections of the pulse sequence that affect the accuracy of the dictionary. The first is the selective excitation for slice selection, which has been a challenging topic because its calculation for the MRF dictionary required high computing resources for solving the Bloch equations. In the initial MRF paper,[1] the dictionary was calculated under the unrealistic assumption that a rectangular cross-sectional region was instantaneously excited. In the next paper published by the same group,[2] the slice selection problem was partly solved using a highly selective excitation pulse (hamming windowed sinc function) with a time-bandwidth (TBW) product of 8. Meanwhile, Hong et al.,[3] showed that slice profile correction was indispensable for an accurate MRF dictionary even for the slice selection pulse with a TBW of 8. Independently, Ma et al.[4] successfully simulated the effects of the slice profile on the dictionary by Bloch simulation of 50 isochromats perpendicular to the slicing plane, including the B_0 offset and B_1^+ entries.

The second section of the pulse sequence is the MRF image data acquisition characterized by the *k*-space trajectory. In the MRF papers published to date, the dictionary was calculated for isochromats that are spatially unresolved in the imaging plane and for the MR signals sampled at a single time point, i.e., the TE. This means that only the MR signal at the origin of the *k*-space was used for dictionary calculation. However, because the T_2 decay temporally changes the MR signal during the data acquisition period, the acquired MRF image depends on how the MR signal was sampled in the *k*-space. Therefore, for MRF dictionary calculation, it is essential to use the Bloch simulation for MR image generation (i.e., Bloch image simulation), which can calculate both the effect of the slice profile and of the *k*-trajectory used for image acquisition.

The new dictionary creation method we propose in this study is that both calculations for slice selection and data acquisition can be performed by a "single" Bloch image simulation for a specially designed dictionary phantom and the

pulse sequence used for the MRF acquisition. This method is accurate and simple because Bloch image simulation software programs are now becoming widely available as described below.

With the recent remarkable increase in the processing speeds of computer systems, various software programs for Bloch image simulation have been reported.[5–9] In particular, with the introduction of graphics processing units (GPUs), a drastic increase in processing speed has been made, and practical Bloch image simulations have become possible, even on a stand-alone PC.[7–9] As a result, Bloch image simulations can play an important role in solving many problems in MRI. In this study, we calculated an entire MR signal throughout the data sampling period, as well as the slice selection period in MRF sequences using a fast Bloch image simulator[8,9] to create accurate dictionaries, and then evaluated the validity of our approach.

Materials and Methods

Pulse sequence design
A standard FISP-based MRF sequence was developed using a 2D FISP sequence composed of a selective excitation pulse (hamming windowed sinc function: $\pm 2\pi$, 6 mm slice thickness) and variable density spiral readout gradients (TE = 3 ms, data acquisition time = 7.47 ms, dwell time = 5 μs, number of readout points = 1494) (Fig. 1). The spiral sequence was designed for 256 × 256 image matrices with a 256 mm square FOV using a design formalism developed by Kim et al.[10] The spiral trajectory with the 0th moment compensation was designed to fill the *k*-space using 48 trajectories, the rotational angles of which were separated by 7.5°. To compare the data sampling trajectory, another MRF sequence with Cartesian sampling (data acquisition time = 1.28 ms, dwell time = 5 μs) having the same selective excitation pulse and the same TE with 0th moment gradient compensation was also developed.

For the MRF signal acquisition 1000 TR units were used, and the TR was randomly varied between 15.0 and 20.0 ms

according to the Perlin noise. The flip angle (FA) was changed as follows:

$$FA = \frac{\pi}{4}\sin\left(\frac{\pi}{200}(i-k)\right) \quad \text{for } 0 \le i \le 200, \, k = 0$$

and for $500 \le i \le 700, \; k = 500,$

and

$$FA = \frac{\pi}{2}\sin\left(\frac{\pi}{200}(i-k)\right) \quad \text{for } 250 \le i \le 450, \, k = 250$$

and for $750 \le i \le 950, \; k = 750$

where *i* is the index number of TR (TR_index), and the FA in other sections was set to zero. The rotational angle of the spiral trajectory was incremented by 120° (*i* = 3*n* and 3*n* + 1, where *n* is an integer) and 127.5° (*i* = 3*n* + 2) in the contiguous TR units to enable the sliding window reconstruction technique.[11] Three contiguous MR signals were used for the reconstruction of one MR image. An inversion pulse was applied 100 ms before the data acquisition sequence to enhance the T_1 contrast of the acquired MR images.

In the MRF pulse sequence for dictionary generation, 48 and 256 repetitions of the MRF pulse sequences were used for the spiral (i.e. full sampling spiral sequence) and Cartesian sampling. In the full sampling spiral sequence, the spiral shots in the MRF pulse sequence were repeated by incrementing the rotation angle by 7.5° to fill the *k*-space. Similarly, the Cartesian sampling in the MRF pulse sequence was repeated while incrementing the Cartesian phase encoding steps. Using this method, 1000 signal datasets filling the *k*-space were acquired, and image reconstruction was performed by inverse nonuniform fast Fourier transform (FFT) and conventional inverse FFT, respectively.

Numerical phantoms
The two numerical phantoms used to evaluate the validity of the dictionary generation method are shown in Fig. 2.
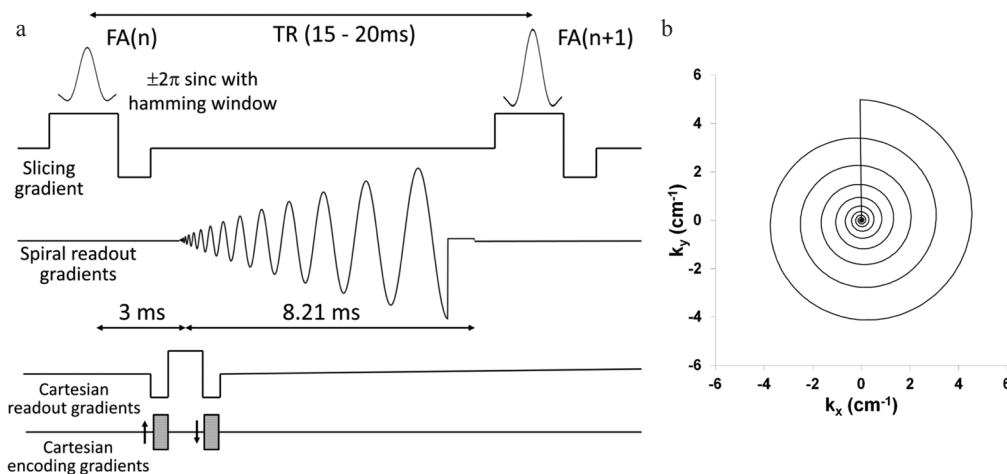

Fig. 1 (**a**) A TR unit of the magnetic resonance fingerprinting (MRF) pulse sequence. The spiral readout gradient was used for dictionary as well as MRF image acquisition. The Cartesian readout gradients were also used for dictionary and MRF image acquisition. (**b**) *k*-trajectory for the spiral readout gradients with 0th moments. FA, flip angle.
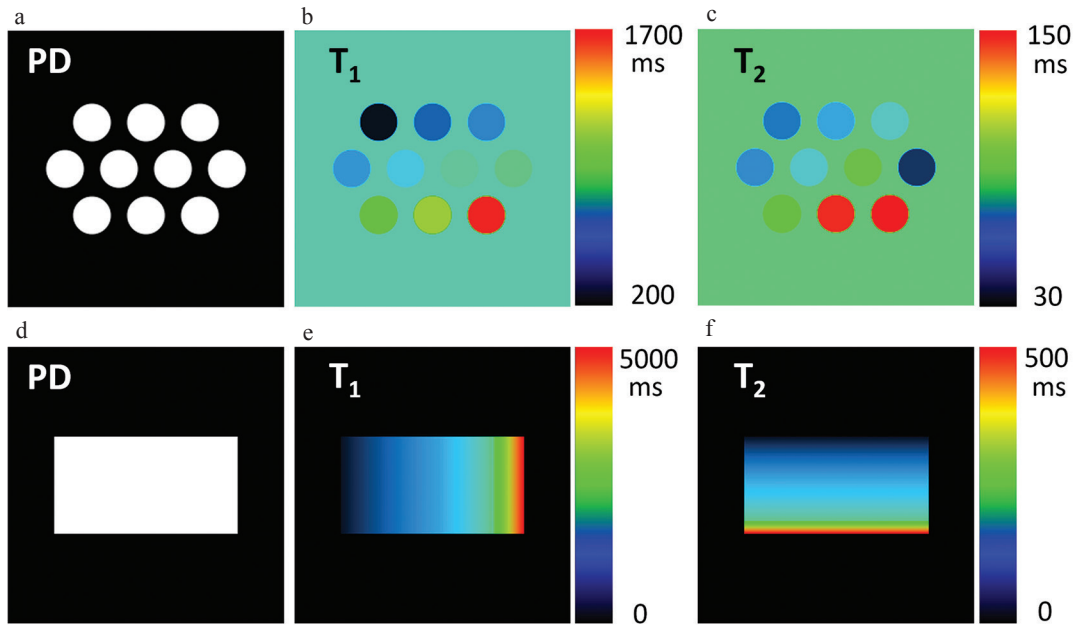
Fig. 2 (**a**–**c**) PD, T_1, and T_2 maps of a numerical phantom with various sets of relaxation times stored in the cylindrical containers (diameter = 35 mm, length = 110 mm). The PDs of the materials were constant, and the combinations of (T_1, T_2) (in ms) were (228, 47), (368, 56), (446, 72), (486, 51), (669, 71), (794, 84), (813, 37), (977, 88), (1227, 146), and (1666, 150). The backgrounds of the bottles in the T_1 and T_2 maps were filled with their average values. (**d**–**f**) PD, T_1, and T_2 maps of a numerical phantom for an magnetic resonance fingerprinting (MRF) dictionary. The phantom was 170 mm wide, 90 mm high, and 110 mm deep. PD, proton density.

The "relaxation time phantom" that simulated 10 cylindrical bottles with the diameter and length of 35 and 110 mm is shown in Fig. 2a and 2c. The bottles were filled with materials having an identical proton density (PD), T_1 ranged from 228 to 1666 ms, and T_2 ranged from 37 to 150 ms. The combinations of T_1 and T_2 were determined from the previous experimental MRF study.[2]

A rectangular dictionary phantom (170 mm wide, 90 mm high, 110 mm deep) filled with materials having identical PD and all possible combinations of relaxation times are shown in Fig. 2d−2f. In the dictionary phantom, T_1 was varied from 100 to 1000 ms by 10 ms steps, from 1000 to 2000 ms by 20 ms steps, and from 2000 to 5000 ms by 100 ms steps, and T_2 was varied from 10 to 200 ms by 2.5 ms steps and from 200 to 500 ms by 25 ms steps.

The parameter values in the numerical phantoms were stored as single-precision floating point numbers in 256^3 matrices having 1 mm^3 voxel size, and were used as input files for the Bloch image simulator described below.

Bloch image simulator

We used a fast Bloch image simulator accelerated by GPUs developed by our group.[8,9] The major advantage of this Bloch image simulator is that it uses the same pulse sequence as that of a real MRI system, and using 32-bit single-precision floating point numbers, effective processing performance of several Tera FLoating point Operations Per Second (TFLOPS) can be realized, even with an inexpensive GPU. In this simulator, static magnetic field inhomogeneity, nonuniformity of the RF magnetic field (transmission: B_1^+ and reception: B_1^-), and

nonlinearity of the gradient magnetic field can be simulated, but these functions were not used in this study.

Bloch image simulation

In the Bloch image simulation, the number of isochromats per voxel is an essential factor for suppressing image artifacts and ensuring calculation accuracy. In the MRF sequence used in this study, the precession phase of isochromats was always refocused in the imaging plane (x–y plane) at the end of the TR. Therefore, in the absence of magnetic field inhomogeneity, one isochromat per voxel within the imaging plane was sufficient. By contrast, considerable phase dispersion of isochromats occurred along the slicing direction (z-direction). Therefore, many isochromats per voxel were required to describe the slice selection profile. In the Bloch image simulation, we used the concept of "subvoxel" and described the phase dispersion by dividing the voxels into subvoxels and allocating one isochromat to each subvoxel.

In the MRF sequence used in this study, the slice thickness was 6 mm, resulting in about six voxels along the z-direction. In the preliminary Bloch image simulation using a varying number of subvoxels (2, 4, 8, and 16) along the z-direction, the correlations between three image sets (subvoxel numbers 2 and 4, 4 and 8, and 8 and 16) were calculated. The correlation between the image set with the subvoxel numbers of 8 and 16 showed a perfect image match, which demonstrated that eight subvoxels were sufficient for the slice profile simulation. Therefore, eight subvoxels per voxel were used along the z-direction, which demonstrated that about 50 isochromats or more were used to describe the

slicing plane. In summary, we divided the FOV into 256 × 256 × 2048 subvoxels and performed Bloch image simulation for the total number of isochromats (13464000) that were included in the dictionary phantom.

In the Bloch image simulation of the MRF sequences, the selective excitation pulse was approximated by 160 square-RF pulses (length = 20 μs), and the sampled signal for the Cartesian and spiral readout gradients were calculated every 5 μs, including the relaxation time effects. These calculations were performed using a GeForce GTX 1070 GPU (peak performance: 6.7 TFLOPS, nVIDIA, Santa Clara, CA, USA) installed on a laptop PC (CPU: Core i7-7700HQ, 16 GB memory).

Pattern matching

The dictionary image datasets acquired with the full sampling spiral and Cartesian sampling sequences were averaged along the TR using three consecutive images for pattern matching. The dictionary image datasets acquired with the spiral sequence were low-pass filtered before pattern matching. As the value of the dictionary changed slowly with respect to the T_1 and T_2 entries of the dictionary, contamination of the T_1 and T_2 values caused by the low-pass filtering (LPF) did not degrade the resolution of the dictionary. Pattern matching was performed using the inner product method. The PD was calculated from the ratios of the time-averaged values for the voxels of the image series acquired with the MRF sequences and those of the matched dictionary entries.

Results

Images of the relaxation time phantom

An image of the relaxation time phantom acquired with the one-shot MRF sequence and reconstructed from three consecutive MR signals is shown in Fig. 3a. This image contains considerable reconstruction artifacts. The temporal changes in the pixel values at the center of the cylindrical samples (S01, S02, and S10) are shown in Fig. 3b. Spike-like abrupt intensity changes were superimposed on the slowly changing

signal caused by the change in the flip angle. The abrupt changes were caused by the image reconstruction artifacts. The simulation time for the one-shot MRF sequence using the relaxation time phantom was about 137 s.

Images of the dictionary phantom

Images selected from the image series of the dictionary phantom that were acquired with the Cartesian and full spiral sampling MRF sequences are shown in Fig. 4a. The simulation times for the dictionary phantom were 5.89 and 2.75 h for the Cartesian and full spiral sampling MRF sequences, respectively. In Fig. 4a, dictionary images displayed on the RGB color scale are shown on the left and bird's-eye view images on the right. For the dictionary phantom acquired with spiral sampling, the bird's-eye views before and after LPF are shown. No noticeable artifacts were seen in the dictionary image by Cartesian sampling, whereas remarkable image reconstruction artifacts appeared on the periphery of the dictionary image by spiral sampling. As the dominant part of the image reconstruction artifacts was from the spatial high-frequency components, LPF was useful for artifacts reduction. Therefore, we used the image dataset obtained from the Cartesian sampling and the low-pass filtered image dataset obtained from the full spiral sampling for pattern matching.

The left and right graphs in Fig. 4b show the temporal changes in the image intensity of the dictionaries obtained from the Cartesian and the full spiral sampling without LPF, respectively. As shown by the arrows, the decrease in image intensity with decreasing T_2 was larger in spiral sampling than in Cartesian sampling. This result was caused by the longer data-acquisition window for spiral sampling (7.47 ms) than for Cartesian sampling (1.28 ms).

Pattern matching results

Pattern matching results (T_1, T_2, and PD maps) for the image datasets of the relaxation time phantom and the two dictionaries, deviation maps from the true values, and correlation plots of the designed and measured values for T_1 and T_2 are
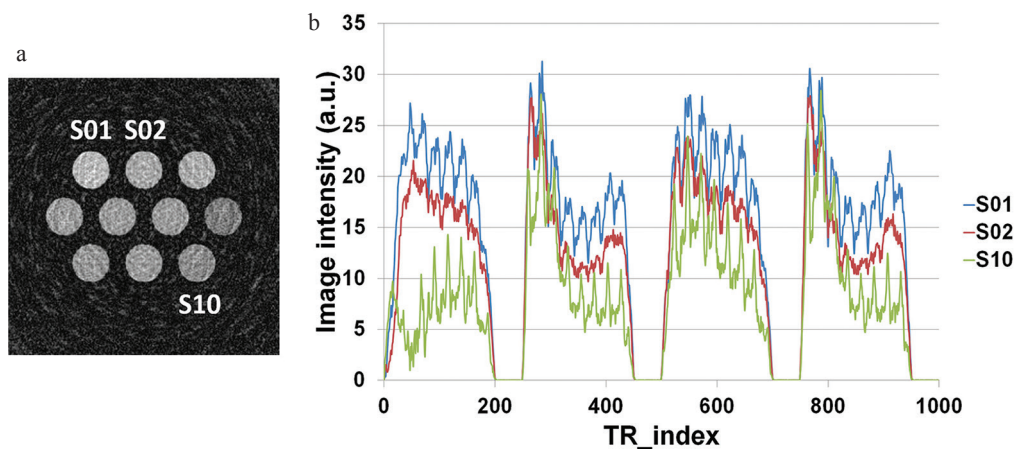

Fig. 3 (**a**) The 280th image of the relaxation phantom reconstructed from three successive spiral shots acquired with a one-shot magnetic resonance fingerprinting (MRF) sequence. (**b**) Image intensity measured at the centers of the S01, S02, and S10 samples versus the TR_index.
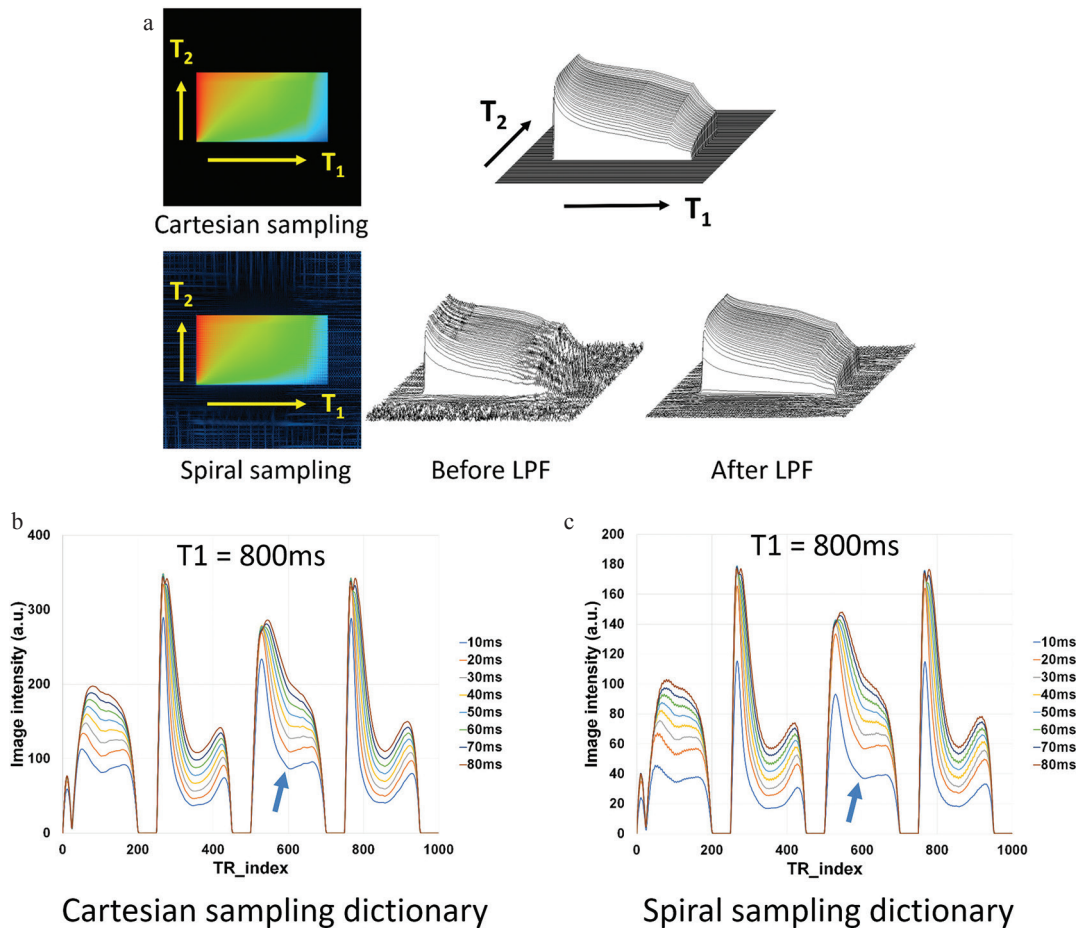
a

T$_2$

T$_1$

Cartesian sampling

T$_2$

T$_1$

T$_2$

T$_1$

Spiral sampling

Before LPF

After LPF

b

Cartesian sampling dictionary

T1 = 800ms

Image intensity (a.u.)

TR_index

—10ms
—20ms
—30ms
—40ms
—50ms
—60ms
—70ms
—80ms

c

Spiral sampling dictionary

T1 = 800ms

Image intensity (a.u.)

TR_index

—10ms
—20ms
—30ms
—40ms
—50ms
—60ms
—70ms
—80ms

Fig. 4 (**a**) The 280th images of the MRF dictionaries acquired with the Cartesian and spiral full sampling magnetic resonance fingerprinting (MRF) sequences. Red, green, and blue (RGB) image (left) and their bird's eyes view (right). (**b**) T$_2$ dependence of the temporal intensity change of the MRF dictionaries acquired with the Cartesian (left) and spiral full (right) sampling MRF sequences without LPF. LPF, low-pass filtering.

shown in Fig. 5a−5d. The Cartesian dictionary was used for pattern matching in Fig. 5a−5c, and the spiral dictionary was used for pattern matching in Fig. 5b−5d. The Cartesian and full spiral sampling image datasets were used in Fig. 5a−5b. The one-shot spiral sampling MRF image dataset was used for Fig. 5c−5d.

The deviation maps in Fig. 5a clearly show that the deviation in T$_1$ and T$_2$ was caused by the lack of resolution of the dictionary entries (T$_1$ and T$_2$) because the deviation maps are homogeneous over the samples. The deviation maps in Fig. 5b clearly show that the deviation in T$_1$ and T$_2$ was caused by the reconstruction artifacts as well as the lack of resolution of the dictionary entries. In Fig. 5c and 5d, where the one-shot MRF sequence was used, the deviations in T$_1$ and T$_2$ were mostly caused by the reconstruction artifacts.

The slopes of the linear regression lines shown in Fig. 5a−5d were 1.0129, 1.015, 0.9453, and 0.9636 for T$_1$ and 0.9945, 1.0128, 0.9375, and 0.9637 for T$_2$, respectively. The slopes were close to unity for the full-sampled MRF images (Fig. 5a and 5b), which demonstrates that the error caused by the MRF simulation and the pattern matching was negligible. For the one-shot MRF images (Fig. 5c and 5d), the differences between 0.9453 and 0.9636 for T$_1$ and that between 0.9375 and 0.9637 for T$_2$ suggest that some

erroneous effects were present in the use of the Cartesian dictionary for the pattern matching of the MRF image dataset acquired by spiral sampling.

Enlarged images of ΔT_2 and the $\Delta T_2/T_2$ plotted against T$_2$ of Fig. 5c and 5d are shown in Fig. 5e and 5f. The overestimation in the T$_2$ value using the Cartesian dictionary in pattern matching was clearly shown by the arrow in the graph. By contrast, the overestimation in the T$_2$ value the spiral dictionary in pattern matching was much less than that using the Cartesian dictionary. These results suggest that the use of identical pulse sequences for both dictionary generation and sample measurement is preferable.

Discussion

Dictionaries by Bloch image simulations and EPG

In this study, two dictionaries generated by the Bloch image simulations were compared using MRF pattern matching. A small but definite difference was observed in the matching results for the samples with short T$_2$ values (37 and 47 ms). As used in the FISP-based MRF sequence, the extended phase graph (EPG) formalism[12] is often used for calculation of the dictionary.[2] The EPG formalism is useful in calculating effects of molecular diffusion as well as those
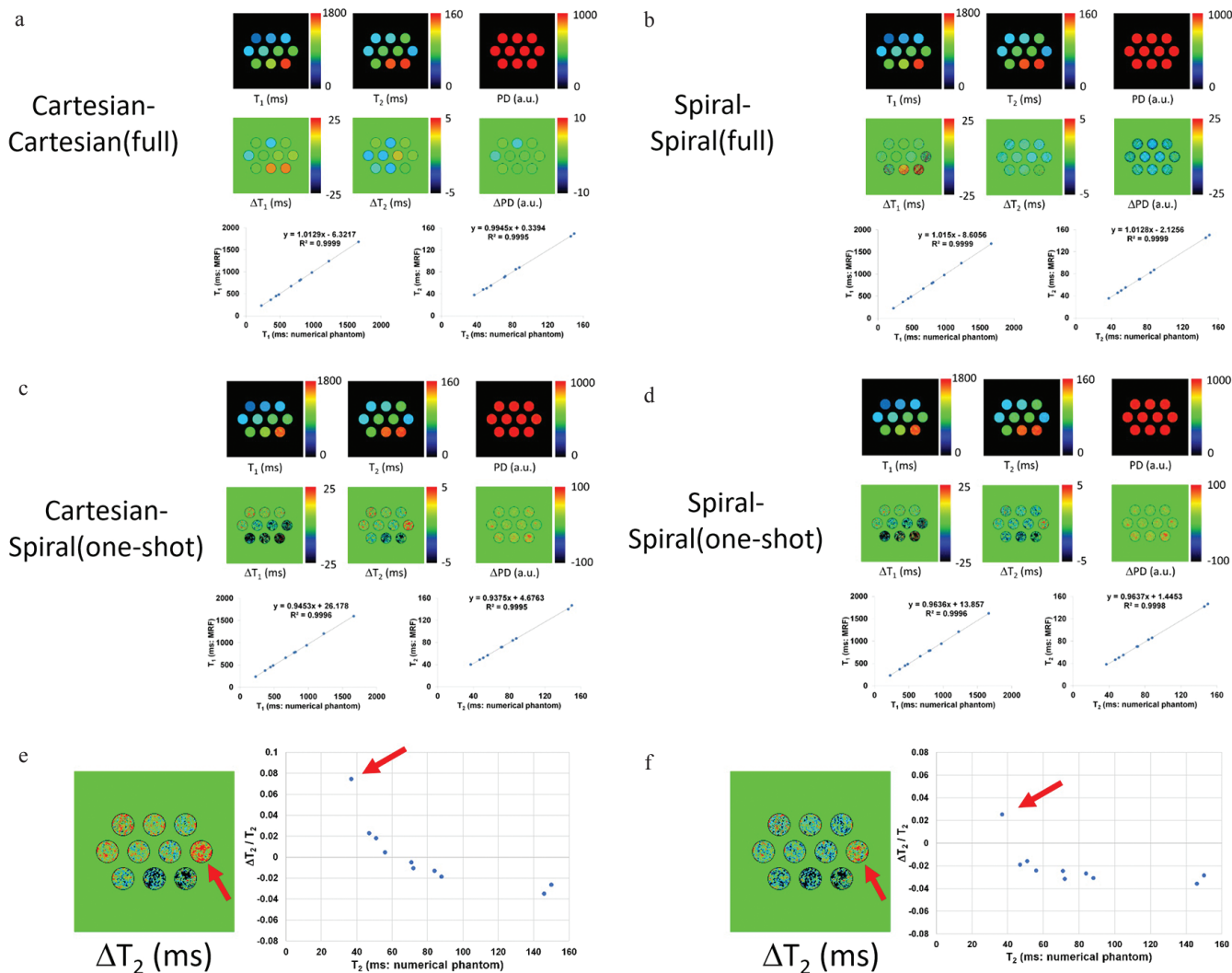
Fig. 5 (**a**–**d**) Matching results (T_1, T_2, and PD maps) for image datasets of the relaxation time phantom and the two dictionaries, deviation maps from the true values, and correlation plots of designed and measured values for T_1 and T_2. The Cartesian dictionary was used for the matching in (**a**) and (**c**) and the spiral dictionary was used for the matching in (**b**) and (**d**). The Cartesian sampling magnetic resonance fingerprinting (MRF) image dataset and the full spiral sampling MRF image dataset were used in (**a**) and (**b**), respectively. The one-shot spiral sampling MRF image dataset was used for (**c**) and (**d**). (**e** and **f**). Enlarged ΔT_2 map and correlations between T_2 and $\Delta T_2/T_2$ for (**c**) and (**d**). PD, proton density.

of relaxation times.[13] However, because the EPG formalism corresponds to a single-point or a constant-time imaging method, the effect of trajectory on the matching result will be observed in a similar manner as in the Cartesian sampling. Therefore, a more accurate dictionary should be constructed using the same trajectory as for the MRF measurement.

Problems in the proposed method
In this section, we discuss three issues, namely, the calculation time for the dictionary, the extension to inhomogeneous static and RF magnetic fields, and the pulse sequence format for Bloch image simulation.

The calculation time required for the dictionary by spiral sampling was 2.75 h. There are two straightforward methods for shortening calculation time: (1) shortening the

depth (110 mm) of the dictionary phantom, and (2) using a high-speed GPU. Because the dictionary phantom was too long for the single slice (6 mm slice thickness) simulation, the length could be shortened to about 10 mm and the calculation time can be reduced to about one-tenth. By introducing a GPU board that is twice as fast as in this study (e.g., GeForce RTX 2080Ti, NVIDIA Corporation, Santa Clara, CA, USA) and installing four GPU boards on a desktop PC, a computing speed that is eight times faster can be easily obtained. In this way, a calculation time shorter by a factor of 80, i.e., about 120 s, could be achieved.

In this study, the dictionary was calculated for a homogeneous static magnetic field and a homogeneous transmitter RF magnetic field. To apply our method to inhomogeneous magnetic field distributions, the dictionary calculation

should be repeated while changing the B_0 and B_1^+ values in 10−20 steps. By unifying the acquired results, an extended dictionary with four entries (T_1, T_2, B_0, and B_1^+) would be obtained for pattern matching.

The proposed method can be implemented in other Bloch image simulators if they have sufficient processing speed and pulse sequence availability. For example, if the MRF sequence is developed using the Pulseq format,[14] the pulse sequence file can be operated on Siemens, Bruker, and GE scanners and used for a JEMRIS Bloch image simulator.[6] However, because the JEMRIS does not operate on a GPU at this time, there might be a problem in calculation speed for a stand-alone PC.

Conclusion

In this study, we proposed a simple and accurate dictionary creation method for MRF using Bloch image simulation and a numerical phantom corresponding to dictionary data. The validity of the generated dictionary was confirmed by MRF simulation and pattern matching using a FISP-based MRF sequence and a numerical phantom containing various relaxation times. By comparing between the two patterns matching results using two different dictionaries acquired with Cartesian and spiral trajectories, we confirmed that the dictionary acquired with the same trajectory as that of the MRF image acquisition produced better matching results. From the above results, we have concluded that the proposed method is useful for MRF dictionary creation.

Conflicts of Interest

Ryoichi Kose and Katsumi Kose are directors of MRIsimulations Inc.

References

1. Ma D, Gulani V, Seiberlich N, et al. Magnetic resonance fingerprinting. Nature 2013;495:187–192.

2. Jiang Y, Ma D, Seiberlich N, Gulani V, Griswold MA. MR fingerprinting using fast imaging with steady state precession (FISP) with spiral readout. Magn Reson Med 2015; 74:1621–1631.

3. Hong T, Han D, Kim MO, Kim DH. RF slice profile effects in magnetic resonance fingerprinting. Magn Reson Imaging 2017; 41:73–79.

4. Ma D, Coppo S, Chen Y, et al. Slice profile and B_1 corrections in 2D magnetic resonance fingerprinting. Magn Reson Med 2017; 78:1781–1789.

5. Benoit-Cattin H, Collewet G, Belaroussi B, Saint-Jalmes H, Odet C. The SIMRI project: a versatile and interactive MRI simulator. J Magn Reson 2005; 173:97–115.

6. Stöcker T, Vahedipour K, Pflugfelder D, Shah NJ. High-performance computing MRI simulations. Magn Reson Med 2010; 64:186–193.

7. Xanthis CG, Venetis IE, Chalkias AV, Aletras AH. MRISIMUL: a GPU-based parallel approach to MRI simulations. IEEE Trans Med Imaging 2014; 33:607–617.

8. Kose R, Kose K. BlochSolver: A GPU-optimized fast 3D MRI simulator for experimentally compatible pulse sequences. J Magn Reson 2017; 281:51–65.

9. Kose R, Setoi A, Kose K. A fast GPU-optimized 3D MRI simulator for arbitrary k-space sampling. Magn Reson Med Sci 2018. doi 10.2463/mrms.mp.2018-0022.

10. Kim DH, Adalsteinsson E, Spielman DM. Simple analytic variable density spiral design. Magn Reson Med 2003; 50:214–219.

11. Cao X, Liao C, Wang Z, et al. Robust sliding-window reconstruction for accelerating the acquisition of MR fingerprinting. Magn Reson Med 2017; 78:1579–1588.

12. Weigel M. Extended phase graphs: dephasing, RF pulses, and echoes - pure and simple. J Magn Reson Imaging 2015; 41:266–295.

13. Kobayashi Y, Terada Y. Diffusion-weighting caused by spoiler gradients in the fast imaging with steady-state precession sequence may lead to inaccurate T_2 measurements in MR fingerprinting. Magn Reson Med Sci 2019; 18: 96–104.

14. Layton KJ, Kroboth S, Jia F, et al. Pulseq: a rapid and hardware-independent pulse sequence prototyping framework. Magn Reson Med 2017; 77:1544–1552.